Photoluminescence from GaN implanted with Be and F

M. A. Reshchikov,[*] O. Andrieiev, M. Vorobiov, and D. O. Demchenko

Department of Physics, Virginia Commonwealth University, Richmond, VA 23220, USA

B. McEwen and F. Shahedipour-Sandvik

College of Nanoscale Science and Engineering, SUNY Polytechnic Institute, Albany NY 12203, USA

Abstract

GaN samples were implanted with Be and F and annealed in different conditions to activate the Be_{Ga} acceptors. Photoluminescence spectra were studied to recognize the defects. The UVL_{Be} band with a maximum at 3.38 eV and the YL_{Be} band with a maximum at 2.15 eV were observed and associated with Be. The sequential implantation of Be and F ions into GaN at 600 °C reduces the concentration of nitrogen vacancies (V_N), as evidenced by the lack of the green luminescence band associated with the isolated nitrogen vacancy. First-principles calculations were employed to find parameters of defects that can form after implantation.

* E-mail: mreshchi@vcu.edu

1. **Introduction**

A renewed interest in doping of GaN with Be is fueled by recent findings that a Be-related acceptor has a level (at 0.113 eV above the valence band) shallower than the currently used Mg_{Ga} acceptor (0.223 eV) and can potentially result in more conductive *p*-type GaN.[1] The shallow Be-related level is responsible for the ultraviolet luminescence (UVL_{Be}) band with a sharp peak at 3.38 eV followed by a few LO phonon replicas in the photoluminescence (PL) spectra.[1] The PL spectra from Be-doped GaN also contain a broad yellow band (YL_{Be}) with a maximum at 2.15 eV. It was recently attributed to the deep (polaronic) state of the Be_{Ga} acceptor.[2] The quantum efficiency of the YL_{Be} band approaches unity in GaN:Be samples grown by metalorganic chemical vapor deposition (MOCVD).[2] Be-doped GaN samples grown by molecular beam epitaxy (MBE) also reveal a green band (GL2) with a maximum at 2.33 eV and a red band (RL_{Be}) with a maximum at 1.8 eV that are attributed to the nitrogen vacancy (V_N) and the V_NBe_{Ga} complex, respectively.[3] The attempts to produce conductive *p*-GaN:Be are rarely successful [4-7] and require confirmation.

Another problem in GaN-based technology is that for realizing vertical GaN power devices local doping and ion implantation is needed. While *n*-type doping via Si-ion implantation is efficient, *p*-type doping by using Mg-ion implantation is more difficult. The Mg-implanted GaN is often high-resistive due to the presence of donors even after post-implantation annealing. Several approaches were suggested to resolve this problem, including ion implantation at high temperatures (800-1000 °C), sequential implantation of Mg and F (or Mg and N) ions into GaN, and annealing under ultrahigh pressure of nitrogen at high temperatures.[8-12] High-temperature implantation reduces implantation damage.[8] The additional implantation with F or N is expected to reduce the concentration of nitrogen vacancies that act as compensating donors.[9,10,12] The V_N can be revealed in PL experiments, where it is associated with the GL2 band.[10,13,14] In particular,

Takahashi *et al*.[9] reported that the GL2 band disappeared when the concentration of implanted F exceeded that of implanted Mg. Note that energy levels of the V_N obtained from analysis of the GL2 band (the 0/+ level at 0.1 eV below the conduction band and the +/3+ level at 0.5-0.7 eV above the valence band) [13,15] agree well with the data obtained from deep-level transient spectroscopy studies of *n*-type and *p*-type GaN irradiated with an electron beam with an energy of 137 keV (0.13 eV and 0.52 eV, respectively).[16,17]

Recently, we investigated PL from GaN implanted with Be and annealed in different conditions.[18] The YL_{Be} band was observed in nearly all the samples, while the UVL_{Be} band appeared only after annealing at high temperatures and ultrahigh nitrogen pressure. One of the goals of the current work is to explore if sequential implantation of GaN with Be and F would suppress the formation of the V_N donors and activate Be-related acceptors, similar to the results achieved with the sequential implantation of Mg and F ions.[9]

First-principles calculations predicted that interstitial fluorine (F_i) is a shallow acceptor in GaN and fluorine substituting for the nitrogen atom (F_N) is a double donor.[19-22] The F_N has low formation energy in *p*-type, while F_i is expected to preferentially form when the Fermi level is closer to the conduction band. Based on these predictions, we expect that the F_N may suppress the formation of the V_N defects, while the F_i may improve *p*-type conductivity. In addition, the $Be_{Ga}F_N$ and other complexes may form unless the migration barriers for the components of complexes are too high for typical temperatures of post-implantation annealing.

Significant diffusion of Be atoms begins at annealing temperatures (T_{ann}) exceeding 1200 °C.[23] Diffusion of fluorine ions in F-implanted GaN begins already at 600 °C, and it is assisted by implantation-induced vacancies.[24] F-vacancy complexes are formed after F implantation and annealing at 600 °C.[25] Implantation at a high temperature is desired not only to reduce the

implantation damage [9] but also to activate Be_{Ga} acceptors. Wahl *et al.*,[26] by using the emission channeling technique, demonstrated that with increasing implantation temperature, Be moves from interstitial position (Be_i) to substitutional (Be_{Ga}), and the fraction of the Be_{Ga} acceptors increases significantly at implantation temperatures above 500 °C.

In this work, we systematically studied PL from GaN implanted at 600 °C with different doses of Be and F and annealed at temperatures from 1100 to 1300 °C. Several PL bands were recognized in the studied material. The experimental results are compared with first-principles calculations using the Heyd-Scuseria-Ernzerhof (HSE) hybrid functional tuned to fulfill the generalized Koopmans' condition.

2. Theory

Figure 1 shows the calculated formation energies of F- and Be-related defects in GaN in N-rich conditions. Among isolated fluorine defects, fluorine substituting for nitrogen, F_N, exhibits the lowest formation energy for Fermi levels lower than about 2 eV above the valence band maximum (VBM). This defect is predicted to be a shallow double donor, and since the shallow defect state wavefunction is too extended to be reproduced in a supercell of a reasonable size, we are unable to predict the energy of the shallow donor level of the F_N. In GaN samples with the Fermi level, E_F, roughly above 2 eV, fluorine interstitial, F_i, calculated here to be a deep acceptor, is energetically favorable. In the neutral charge state, this defect exhibits multiple metastable geometries around the wurtzite cage center. We find at least three non-equivalent lattice structures of neutral F_i, one stable neutral ground state, and two metastable lattice structures with energies 0.21 and 0.38 eV above the ground state. Only one stable singly negative charge state could be found. The lowest-energy neutral state creates a deep acceptor level at 0.64 eV above the VBM (Figure 1), while metastable states have 0/- transition levels at 0.43 and 0.26 eV above the VBM.

Calculated configuration coordinate diagrams (not shown here) suggest that the F_i is a non-radiative recombination center. Therefore the lowest-energy isolated F-related defects are not expected to be observed in PL experiments.

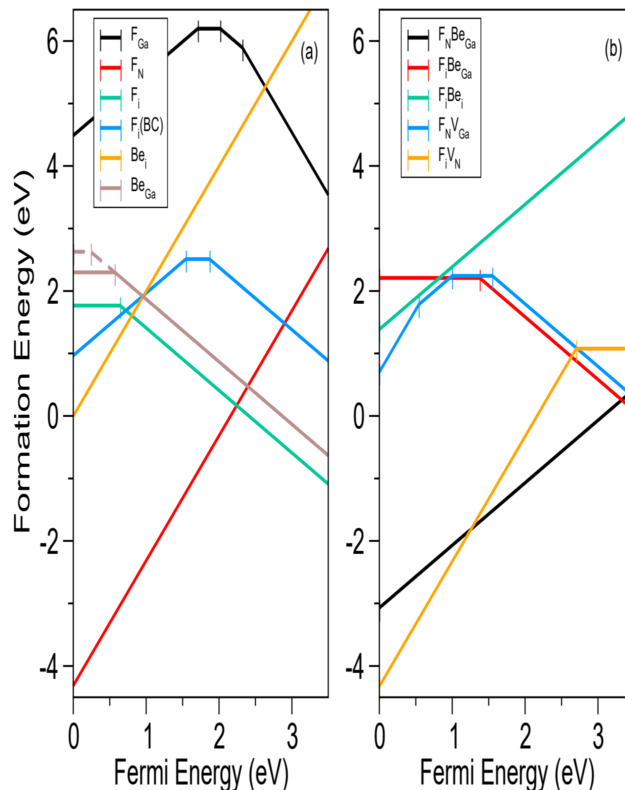

Figure 1. Calculated formation energies of F- and Be-related defects in GaN. N-rich conditions are assumed. (a) Isolated F and Be defects; (b) F- and Be-containing complexes. Transition levels are indicated with vertical ticks.

In addition to the F-interstitial around the wurtzite cage center, we also find a stable bond-center F-interstitial (shown as $F_i(BC)$ in Figure 1), where the F atom is in the middle of the Ga-N bond, pushing Ga and N atoms significantly far apart and stretching the Ga-N distance from the equilibrium bond length of 1.97 Å to 3.74 Å. In this configuration, the $F_i(BC)$ exhibits both donor +/0 and acceptor 0/- levels, at 1.54 eV and 1.87 eV, respectively, above the VBM. Transitions via

both +/0 and 0/- levels of F_i(BC) are also predicted to be non-radiative. Finally, fluorine substituting gallium atom, F_{Ga}, exhibits significantly higher formation energies, by about 5 eV and more (depending on the Fermi energy), and therefore is unlikely to form.

As reported in our previous work,[3,27] in its lowest energy isolated Be forms Be_{Ga} acceptor and Be_i interstitial double donor. The Be_i is favorable in *p*-type GaN, while the Be_{Ga} acceptor is favorable for Fermi energies above about 1 eV. The Be_{Ga} acceptor in the neutral charge state is predicted to have dual nature, where the ground state of the hole localized on the acceptor forms a deep polaronic state, computed with the current parametrization of HSE at 0.5 eV above the VBM, while a shallow state of the hole is at 0.23 eV above the VBM[1] (shown with a dashed line in Figure 1). The competition between the double donor Be_i and acceptor Be_{Ga} during sample growth or annealing at high temperatures (~1300 °C) suggests likely self-compensation of Be-doped samples.

HSE calculations also predict that the formation of stable F- and Be-complexes is possible in co-implanted GaN samples, as shown in Figure 1. Among these complexes, F_NBe_{Ga} and F_iBe_i are shallow donors and would not contribute to a PL signal. They, however, can act as compensation centers detrimental to possible *p*-type doping by Be. The F_iBe_i complex has a relatively high formation energy and binding energy of 1 eV at most Fermi levels. The F_NBe_{Ga} is favorable for Fermi energies higher than about 1 eV above the VBM, and a binding energy of 1.6 eV for most E_F. In *p*-type samples (i.e., for $E_F < 0.5$ eV), binding energies of these complexes decrease to 0.4 and 1 eV for the F_iBe_i and F_NBe_{Ga}, respectively. Once the formation of complexes is taken into consideration, fluorine interstitial acceptor F_i becomes energetically favorable only for E_F above 2.8 eV. The F_iBe_{Ga} is a deep acceptor, that is found to be bound only for $E_F < 1.5$ eV, while for Fermi levels above this value, this complex is unstable due to the repulsive Coulomb

interaction between two acceptor constituents. It should be noted that this complex was calculated by lattice relaxation of a donor-acceptor complex $F_{Ga}Be_i$ as a starting point. However, upon relaxation F atom moves away from the Ga site to the interstitial, while Be atom moves into it. As a result, similar to isolated F_i defect, this complex also exhibits multiple metastable lattice configurations in both neutral and singly negative charge states. Deep acceptor levels for various configurations of the F_iBe_{Ga} complex vary between 1.30 eV and 1.65 eV above the VBM (Figure 1 shows the transition level between the lowest energy configurations of F_iBe_{Ga}). Two remaining complexes considered here are those of F with native vacancies that could be formed during implantation. As such, the F_NV_{Ga} forms both deep acceptor and deep donor transition levels, i.e., $E(2+/+) = 0.54$ eV, $E(+/0) = 1.0$ eV, $E(0/-) = 1.55$ eV. The F_iV_N complex is a negative-U deep donor with +/0 and 2+/+ levels at 2.58 eV and 2.83 eV, respectively (the U value of -0.25 eV). While the F_NV_{Ga} has a higher formation energy, the F_iV_N has a formation energy very similar to that of a shallow double-donor F_N. The binding energy of the F_NV_{Ga} varies from about 1 eV for E_F around the VBM to 4.3 eV for $E_F > 2.5$ eV. The binding energy of F_iV_N is 6.5 eV for E_F close to the VBM and decreases almost linearly to ~2 eV in *n*-type samples. Overall, formation energies of F- and Be-related defects in GaN suggest that donor defects, both shallow and deep, will form predominantly (F_N, F_iV_N, F_NBe_{Ga}), except for in *n*-type samples, where F_i acceptors are energetically favorable. This suggests that, although fluorine co-doping would suppress the formation of nitrogen vacancies V_N, fluorine and its complexes tend to form donors as well, therefore unlikely to improve *p*-type doping of GaN.

3. Experimental Results

3.1. General trends

We reported previously [18] that in undoped GaN implanted with Be (with AlN cap) and annealed in N_2 ambient at 1100 °C, a strong Be-related YL_{Be} band appeared. The V_N-related GL2 band could be resolved in almost all of these samples at low excitation intensity (P_{exc}) at temperatures between 200 and 250 K when the YL_{Be} band was quenched.

In all GaN samples grown by hydride vapor phase epitaxy (HVPE) and co-implanted with Be and F and annealed at temperatures between 1100 and 1300 °C (Table 1), the Be-related YL_{Be} band is strong, with the internal quantum efficiency (IQE) higher than 0.1 (will be discussed in Section 3.3). The Be-related UVL_{Be} band with a maximum at 3.38 eV could be resolved in 4 samples (series E) out of 36 samples (Section 3.4).

Table 1. Parameters of GaN samples after ion implantation

Sample series	Sample name	^{9}Be dose (cm^{-2})	^{19}F dose (cm^{-2})	[Be] a) (cm^{-3})	[F] a) (cm^{-3})	[Be] SIMS	[F] SIMS
A	u,Si-12-11-T_{ann}	10^{12}	10^{11}	5×10^{16}	7×10^{15}		
B	u,Si-12-12-T_{ann}	10^{12}	10^{12}	5×10^{16}	7×10^{16}		
C	u,Si-12-13-T_{ann}	10^{12}	10^{13}	5×10^{16}	7×10^{17}		
D	u,Si-13-12-T_{ann}	10^{13}	10^{12}	5×10^{17}	7×10^{16}		
E	u,Si-13-13-T_{ann}	10^{13}	10^{13}	5×10^{17}	7×10^{17}	5×10^{17}	$<10^{18}$
F	u,Si-13-14-T_{ann}	10^{13}	10^{14}	5×10^{17}	7×10^{18}	1×10^{18}	10^{18}-10^{19}
G	u,Si-13-T_{ann}	–	10^{13}	–	7×10^{17}		

a) The average concentrations of Be and F in the near-surface 150 nm-thick layer (from which PL signal is collected) are estimated from TRIM simulations.

A weak blue band was observed in almost all samples intentionally doped with Si before the ion implantation. The shape and position of this band were similar to those of the Zn_{Ga}-related BL1 band, yet its relative intensity was too weak for reliable identification. A very weak Mg_{Ga}-related

UVL_{Mg} band with the first peak at 3.27 eV was observed in some samples (both undoped and Si-doped). The C_N-related YL1 band was found in some samples at temperatures above 200 K when the YL_{Be} band was quenched. In undoped GaN implanted with F, the YL1 band was strong due to contamination with C during MOCVD growth. We attribute the YL1, BL1, and UVL_{Mg} bands in the studied samples to contamination of the HVPE-grown GaN with C, Zn, and Mg impurities, respectively. Note that very low concentrations of C, Zn, and Mg (even below the detection limits of SIMS) may cause strong PL bands in undoped and Si-doped GaN samples because these acceptors efficiently capture free holes.[28]

In samples, undoped before the ion implantation, where the concentration of F exceeded that of Be (u-12-13 and u-13-14 annealed at different temperatures), a new orange luminescence (named OL1) band with a maximum at 1.9 eV could be resolved (Section 3.5). The same PL band could be resolved in GaN implanted with only F. In Si-doped GaN, after ion implantation with F and Be ([F] > [Be]), a red luminescence band (labeled RL5) appeared with a maximum at about 1.5 eV. Apparently, the same RL5 band was observed in GaN implanted with only F. The V_N-related GL2 band was found only in five samples, and all these samples were semi-insulating (undoped GaN from series D and E). It was weaker than the YL_{Be} band and could be resolved only after the YL_{Be} band was quenched at temperatures between 150 and 250 K.

In general, Si-doped GaN implanted with different doses of Be and F were conductive *n*-type, while undoped GaN implanted and annealed in the same conditions were often semi-insulating. We could distinguish *n*-type conductivity from semi-insulating by studying the temperature dependence of PL intensity and PL lifetime (Sections 3.3 and 3.4).

3.2. Shapes of PL bands

Figure 2 shows low-temperature PL spectra from two representative samples. Sample Si-12-12-1200 is Si-doped GaN implanted with Be and F with doses of 10^{12} cm^{-2} and annealed at 1200 °C. Sample u-13-13-1200 is undoped GaN implanted with Be and F with doses 10^{13} cm^{-2} and annealed at 1200 °C. The samples are conductive *n*-type and semi-insulating, respectively. The exciton emission (with the main peak at 3.475 eV) in sample Si-12-12-1200 is strong and increases linearly with P_{exc}. In sample u-13-13-1200, it is much weaker and increases super-linearly with P_{exc}, which is typical for semi-insulating GaN.[28] In both samples, the YL_{Be} band is the strongest defect-related PL band.

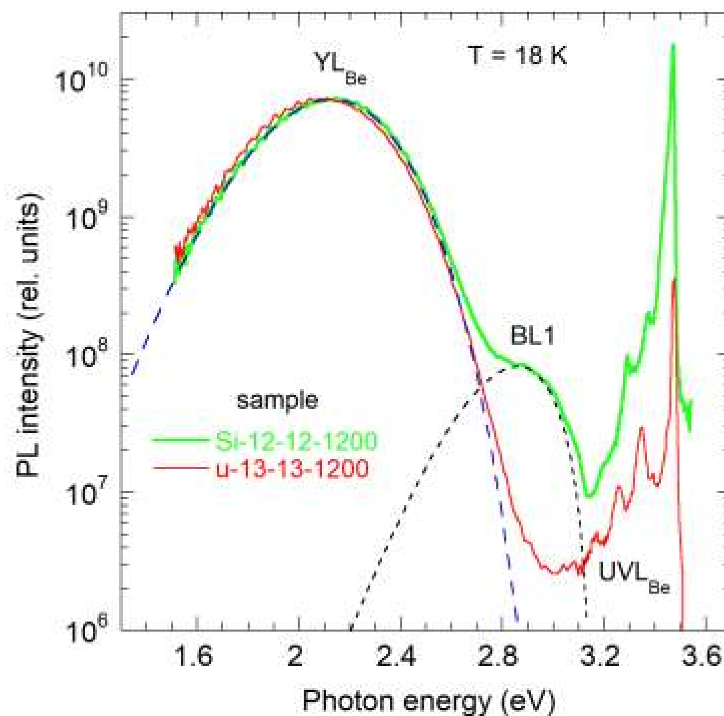

Figure 2. PL spectra from GaN co-implanted with Be and F. $T = 18$ K and $P_{exc} = 10^{-4}$ W/cm^2. The PL spectra are measured in identical conditions and plotted in relative units. The dashed lines are calculated using Eq. (1) with parameters in Table 2 and $\Delta = -0.02$ eV for the YL_{Be} band and $\Delta = 0$ for the BL1 band. For sample u-13-13-1200, the UVL_{Be} band is well resolved, with the main peak at 3.38 eV.

The shapes of broad defect-related PL bands were fitted with the following expression obtained in a one-dimensional configuration coordinate model [13]

$$I^{PL}(\hbar \qquad \hbar \qquad \left[-2S_e \left(\sqrt{\frac{E_0^* - \hbar}{d_{FC}^g}} \quad 1 \right)^2 \right]. \qquad (1)$$

Here, S_e is the Huang-Rhys factor in the excited state of the defect, $d_{FC}^g = E_0^* - \hbar$ is the Franck-Condon shift in the ground state, $E_0^* = E_0 + 0.5\hbar$, E_0 is the zero-phonon line (ZPL) energy, $\hbar$ is the energy of the effective phonon mode in the excited state, $\hbar$ and $\hbar$ are the photon energy and position of the PL band maximum, respectively. The Δ is a small shift of the PL band maximum due to sample-dependent reasons such as in-plane biaxial strain in thin GaN layers grown on sapphire substrates. Since $\hbar\omega_{max}$ is not a fitting parameter, the shape of a PL band depends only on S_e and E_0^* .

In order to deconvolute PL spectra where several PL bands overlap (Figure 2), the shapes of broad defect-related PL bands in this study were fitted using Eq. (1) with parameters found previously from high-quality GaN samples where the overlaps are insignificant, and the distortions of the PL band shapes and positions due to different reasons are negligible.[28] The parameters are given in Table 2.

Table 2. Defect-related PL bands in studied GaN samples and parameters in Eq. (1) defining the bands' positions and shapes

PL band	Attribution	$\hbar\omega_{max}$ (eV)	E_0^* (eV)	S_e	d_{FC}^g (eV)
BL1	Zn_{Ga}	2.86	3.14	3.0	0.28
YL1	C_N	2.17	2.67	7.8	0.50
YL_{Be}	Be_{Ga}	2.15	3.2	21-22	1.05
OL1	F_NV_{Ga}?	1.88	2.53	10-11	0.65

3.3. The Yellow (YL_{Be}) Band

3.3.1. The Effect of Temperature

The shape of the YL_{Be} band can be fitted using Eq. (1) with the same parameters (Table 2) as for the YL_{Be} band in Be-doped GaN grown by MBE, MOCVD, and in Be-implanted GaN.[2,3,18,29] The band maximum in semi-insulating GaN samples red-shifts by up to 60 meV with decreasing P_{exc} from 0.1 to 10^{-5} W/cm^2. As in the case of Ca-implanted GaN,[30] the shift can be caused by local electric fields in semi-insulating GaN.[28,31]

The characteristic feature of the YL_{Be} band is the two-step quenching with increasing temperature.[2,3,29] This effect was observed in all samples without exception. Temperature dependences of the YL_{Be} intensity for two representative samples (normalized at T = 18 K) are shown in Figure 3. In a conductive *n*-type sample (Si-13-13-1300), the first step of the quenching begins at T = 90 K, and the second step at 170 K. The quenching is not tunable by excitation intensity; i.e., the normalized $I^{PL}(T)$ dependences for different P_{exc} coincide. For transitions from the conduction band to the defect level in an *n*-type semiconductor, the $I^{PL}(T)$ dependence can be fitted with the following expression:[28]

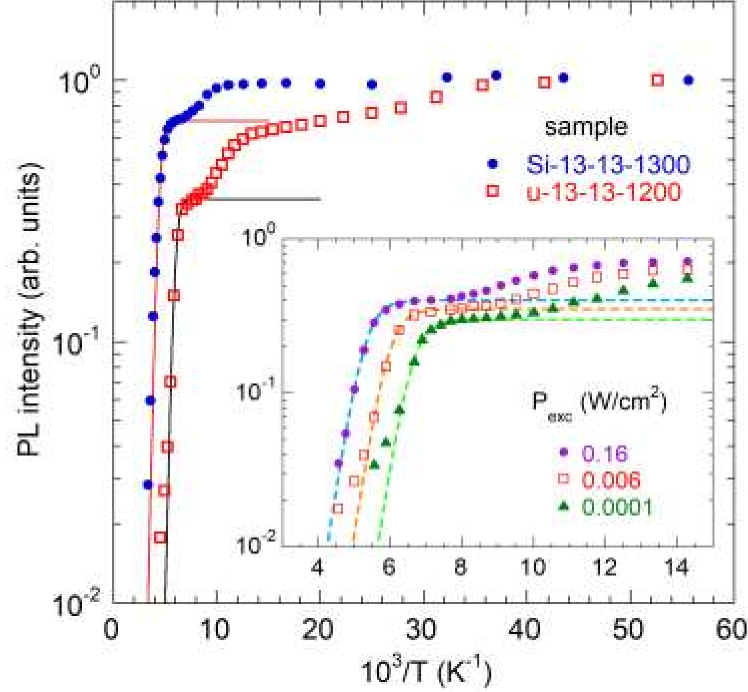

Figure 3. Normalized temperature dependence of the YL_{Be} intensity in *n*-type (Si-13-13-1300) and semi-insulating (u-13-13-1200) GaN:Be,F samples. $P_{exc} = 0.006$ W/cm^2. The solid lines are calculated using Eq. (2) with the following parameters: $(1-\eta_0)C_p\tau_0 = 1\times10^{-12}$ cm^3 (sample Si-13-13-1300) and $(1-\eta_0)C_p\tau_0 = 3\times10^{-10}$ cm^3 (sample u-13-13-1200). $E_A = 0.30$ eV and $N_{v1} = 3.5\times10^{15}$ cm^{-3}K$^{-3/2}$ for both samples. The inset shows the region of the first and second quenching steps for sample u-13-13-1200 at selected P_{exc}. The dashed lines are calculated using the following equation: $I^{PL}(0)/I^{PL}(T)=1+C\exp(-E_A/kT)$ with $C = 10^8$, 10^9, and 10^{10} for $P_{exc} = 0.16$, 0.006, and 1×10^{-4} W/cm^2, respectively, and $E_A = 0.30$ eV for all three curves.

$$I^{PL}(T) = \frac{I^{PL}(0)}{1+(1-\eta_0)\tau_0 C_p N_v g^{-1}\exp\left(\frac{-E_A}{kT}\right)}. \tag{2}$$

Here, $I^{PL}(0)$, η_0 and τ_0 are the PL intensity, IQE, and PL lifetime, respectively, at temperatures before the quenching begins, N_v is the effective density of states in the valence band (we assumed $N_v = N_v' T^{3/2}$ with $N_v' = 3.15\times10^{15}$ cm^{-3}K$^{-3/2}$ for GaN), k is Boltzmann's constant; g is the degeneracy of the defect level (assumed $g = 2$), C_p is the hole-capture coefficient for the defect, and E_A is the

defect ionization energy (the distance from the defect level to the valence band). The parameters E_A and C_p for the YL_{Be}-related defect were found from analysis of Be-doped GaN grown by MBE,[3] and the PL lifetime τ was directly measured with time-resolved PL (TRPL). The most significant error in this fit with known E_A and C_p may originate from the uncertainty in η_0. Nevertheless, $\eta_0 = 0.25$ from the best fit shown in Figure 3 is a reasonable value.

In semi-insulating GaN (u-13-13-1200), the first and second quenching steps are tunable by excitation intensity. The inset in Figure 3 shows that the critical temperatures of the first and second quenching shift to higher temperatures with increasing P_{exc}. The behavior is identical to the behavior of the YL_{Be} band in semi-insulating GaN:Be grown by MBE and MOCVD.[2,3] In this case, the $I^{PL}(T)$ dependence can be formally fitted by Eq. (2), yet the parameters of the fit do not have physical meaning, and their values may appear unreasonable.[28,43] Note that the value of E_A = 0.30 eV obtained from the quenching of PL in the semi-insulating sample is accidentally close to the value obtained from conductive n-type GaN:Be or GaN:Be,F samples. In other semi-insulating samples, the slope of the quenching was more abrupt.

3.3.2. Time-resolved PL

The lifetime of PL caused by transitions from the conduction band to a defect level in an n-type semiconductor is equal to

$$\tau = \frac{1}{C_n n}, \tag{3}$$

where C_n is the electron-capture coefficient and n is the concentration of free electrons.[28,32] The C_n is a parameter of the defect showing how efficiently the defect captures electrons. Previously, from about 20 Be-doped GaN samples grown by MBE, we found only one conductive n-type sample, with $\tau = 25$ μs and $n \approx 4\times10^{17}$ cm^{-3} at $T = 200$ K, from which we estimated $C_n = 1\times10^{-13}$

cm^3/s for the YL_{Be}-related defect.[3] The same value was found for the YL_{Be} band in conductive GaN:Be sample grown by MOCVD.[2] For samples implanted with Be and F, the n cannot be reliably found from the Hall effect measurements because the conductive GaN:Si material beyond the implanted region shunts the current. However, in some samples, the YL_{Be} band was observed together with the Mg-related UVL_{Mg} band, and the PL lifetimes of these bands could be compared. For example, for samples Si-12-11-1100 and Si-13-12-1100, $\tau = 10$ μs for the YL_{Be} band and $\tau = 0.3$ μs for the UVL_{Mg} band at $T = 100$ K. With known C_n for the UVL_{Mg} band (3.2×10^{-12} cm^3/s),[33] we find from Eq. (3) that $n = 1.0\times10^{18}$ cm^{-3} and $C_n = 1\times10^{-13}$ cm^3/s for the YL_{Be} band. With known C_n for the YL_{Be} band, after measuring its lifetime in other samples, we determined that the typical concentration of free electrons in the implanted region is 10^{18} cm^{-3} for Si-doped GaN samples.

3.4. The Ultraviolet (UVL_{Be}) Band

3.4.1. The UVL_{Be} Band in Semi-insulating GaN

The Be-related UVL_{Be} band was relatively strong in only one sample (u-13-13-1200). The IQE of the YL_{Be} and UVL_{Be} bands in this sample are estimated as 0.4 and 5×10^{-4}, respectively. At $T = 18$ K, the first peak of the UVL_{Be} band at 3.36 eV is followed by three LO phonon replicas. The evolution of the PL spectrum with temperature is shown in Figure 4. The donor-bound exciton (DBE) and free exciton (FE) peaks are at 3.477 and ~3.483 eV, respectively, in that sample at $T = 18$ K (not shown). The LO phonon replicas of these peaks can be observed at lower photon energies. A characteristic transformation of the UVL_{Be} band shape with temperature is observed.[1,3] The donor-acceptor-pair (DAP) components gradually disappear, and the components due to transitions from the conduction band to the same acceptor level emerge (the eA transitions with ZPL at 3.38 eV shown with dotted lines in Figure 4). The quenching of the eA

components begins at 70 K, and the band completely disappears at $T > 110$ K. A band with the first peak at ~3.28 eV is identified as the Mg-related UVL_{Mg} band (Figure 4).[28] The quenching of both the YL_{Be} and UVL_{Be} bands in this sample is tunable by excitation intensity; i.e., the critical temperature at which the quenching begins to increase with increasing P_{exc}. This behavior indicates that the sample is semi-insulating.[28,29]

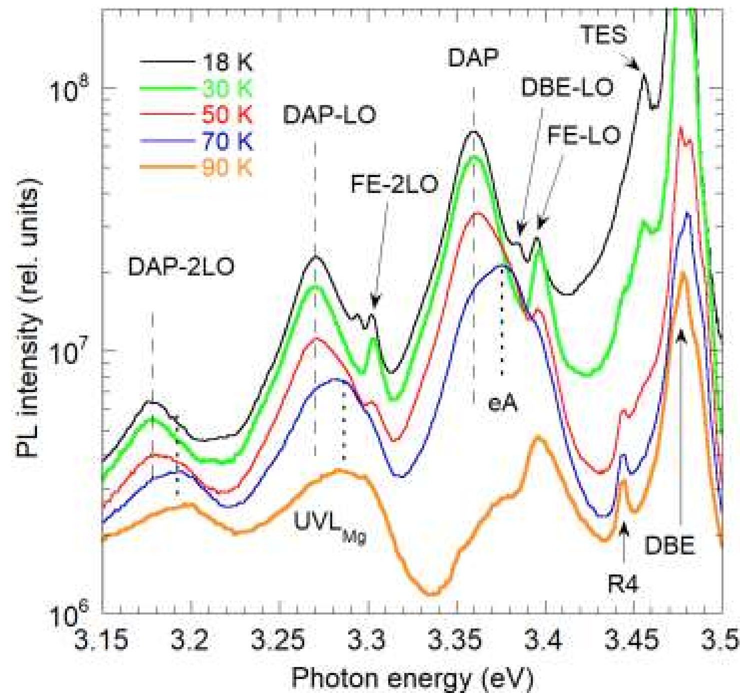

Figure 4. Evolution of PL spectrum with temperature for semi-insulating GaN:Be,F (sample u-13-13-1200). $P_{exc} = 0.16$ W/cm^2. The DAP and eA components of the UVL_{Be} band are shown with dashed and dotted vertical lines, respectively. The *R*4 peak is the resonance Raman line. The TES is the two-electron satellite of the DBE line.

3.4.2. The UVL_{Be} Band in Conductive n-type GaN

In three other samples (u-13-13-1300, Si-13-13-1200 and Si-13-13-1300) the UVL_{Be} band could not be reliably identified at $T = 18$ K but can be resolved after the exciton emission is partly quenched at elevated temperatures. This is the first observation of the UVL_{Be} band in *conductive* *n*-type GaN (samples Si-13-13-1200 and Si-13-13-1300). The steady-state PL (SSPL) spectra at *T*

= 18 and 50 K for one of these samples (Si-13-13-1300) are shown in Figure 5. The peak at 3.472 eV is attributed to the exciton emission, whereas the peak at 3.374 eV, followed by LO phonon replicas, is the UVL_{Be} band. The PL spectrum taken at 300 ns after a laser pulse in the TRPL experiment coincides with the SSPL spectrum.

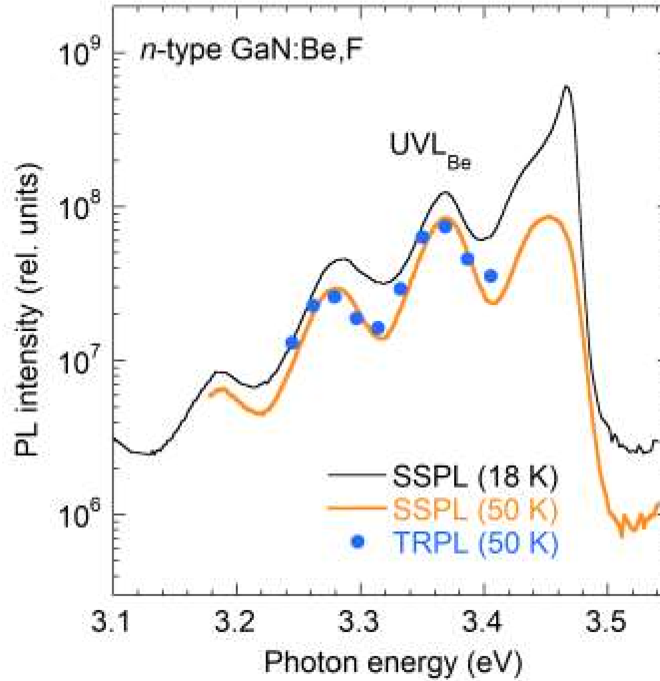

Figure 5. SSPL spectra at T = 18 and 50 K ($P_{exc} \approx 10$ W/cm^2) from n-type GaN:Be,F sample Si-13-13-1300 ($n \approx 7\times10^{17}$ cm^{-3} at 50 K). The empty circles show the TRPL spectrum at a time delay of 300 ns and T = 50 K.

The PL lifetimes for the UVL_{Be} and YL_{Be} bands in this sample are 0.15 μs and 15 μs, respectively, independent of temperature between 18 and 80 K. The quenching of these bands (in SSPL experiments) is not tunable, indicating that the sample is conductive n-type. The concentration of free electrons at T = 50 K is estimated at ~7×10^{17} cm^{-3} from $C_n = 1\times10^{-13}$ cm^3/s for the YL_{Be} band (Section 3.3.2). The ratio $\tau_{YL}/\tau_{UVL} = C_n^{UVL}/C_n^{YL}$ is about 100. The same ratio was obtained for effective lifetimes of the YL_{Be} and UVL_{Be} bands in semi-

insulating MBE-grown GaN:Be (sample 0408b) with $\tau_{YL} \approx 10^{-4}$ s and $\tau_{UVL} \approx 10^{-6}$ s.[3] However, in that work, we were unable to find the C_n because the sample was semi-insulating. By taking $C_n = 1\times10^{-13}$ cm^3/s for the YL$_{Be}$ band, we conclude that $C_n \approx 1\times10^{-11}$ cm^3/s for the UVL$_{Be}$ band.

3.4.3. Concentrations of Defects Responsible for the UVL$_{Be}$ and YL$_{Be}$ Bands

Figure 6 shows the temperature dependence of the UVL$_{Be}$ band intensity in two samples. The PL quenching begins at $T \approx 60$ K. The quenching is not tunable by the excitation intensity, which supports the assumption that the Si-doped GaN samples remain conductive n-type after implantation with Be and F.

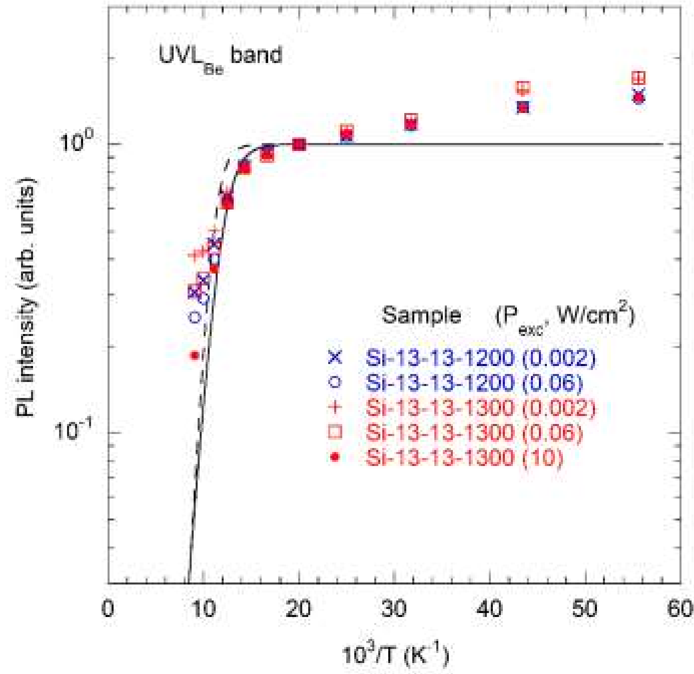

Figure 6. Normalized temperature dependence of the UVL$_{Be}$ intensity in n-type GaN:Be,F (samples Si-13-13-1200 and Si-13-13-1300). The lines are calculated using Eq. (2) with the following parameters: $(1-\eta_0)C_p\tau_0 = 1.5\times10^{-14}$ cm^3 and $E_A = 0.07$ eV (solid line) and $(1-\eta_0)C_p\tau_0 = 3\times10^{-13}$ cm^3 and $E_A = 0.10$ eV (dashed line). $N_{v1} = 3.5\times10^{15}$ cm^{-3}K$^{-3/2}$ for both fits.

Note that the intensity of the UVL_{Be} band could not be traced at temperatures above 110 K because the band disappears under the tail of the exciton emission. As a result, the points at 100 and 110 K have considerable uncertainty. In such a situation, the fit with Eq. (2) may lead to significant errors in C_p and E_A. To reduce the errors, we fixed the E_A based on the following arguments. In the fit of experimental $I^{PL}(T)$ dependences for defects in n-type GaN, the E_A is about 83-91% from the E_A determined from the ZPL at T = 15-18 K (186, 340, and 835 meV versus 223, 400, and 916 meV for the UVL_{Mg}, BL1, and YL1 bands, respectively).[28] The lower value of E_A in these examples is not a mistake of the fit (the quenching region extends for more than three orders of magnitude) and can be caused by at least two reasons. First, the energy level splits into a band due to the high concentration of impurities, and the thermal emission starts from the closest to the valence band levels. Another reason is that the acceptor ionization energy decreases with increasing temperature. For example, first-principles calculations predict that the E_A for the C_N defect decreases from 1.04 to 0.94 eV with increasing temperature from 0 to 600 K.[34]

Thus, it is reasonable to assume E_A = 0.10 eV instead of 0.113 eV for the UVL_{Be} band at temperatures of its quenching. The fit with this E_A is shown with a dashed line in Figure 6. However, the E_A may be even smaller since the overlap of hole wavefunctions for such a shallow acceptor is significantly larger than that for the Mg_{Ga}, Zn_{Ga}, and C_N acceptors. By analyzing PL quenching of the UVL_{Be} band in semi-insulating GaN:Be grown by MBE (where PL intensity decreased by more than two orders of magnitude), we have found E_A = 0.070 eV. The fit with this E_A is shown with a solid line in Figure 6. By using τ = 0.15 μs from TRPL and $(1-\eta) = 1$, we find $C_p = 1\times10^{-7}$ cm^3/s if E_A = 0.070 eV and $C_p = 2\times10^{-6}$ cm^3/s if E_A = 0.10 eV. The value of C_p in the range of $(1\text{-}20)\times10^{-7}$ cm^3/s agrees with the C_p for acceptors in GaN (from 3.7×10^{-7} cm^3/s for the C_N-related YL1 band to 1×10^{-6} cm^3/s for the Mg_{Ga}-related UVL_{Mg} band).[28] Finally, taking

into account the fact that the PL intensity in *n*-type GaN is proportional to C_pN, where N is the defect concentration,[28,35] and the integrated intensity of the YL_{Be} band (with $C_p \approx 4\times10^{-7}$ cm^3/s)[3] is typically by at least 2-3 orders of magnitude higher than that for the UVL_{Be} band, we conclude that the concentration of the YL_{Be}-related defect is at least 2-3 orders of magnitude higher than the concentration of the UVL_{Be}-related defect in Be-doped and Be-implanted GaN samples.

3.5. Other PL Bands

3.5.1. The Orange (OL1) Band in Semi-insulating GaN:Be,F

In PL spectra from five out of six undoped GaN samples where the concentration of F significantly exceeds that of Be (u-12-13 and u-13-14 annealed at 1100, 1200, and 1300 °C), we observed a contribution of a new broad PL band with a maximum at 1.9 eV (labeled OL1). Figure 7 shows PL spectra at selected P_{exc} for sample u-12-13-1100. By subtracting the YL_{Be} band from the

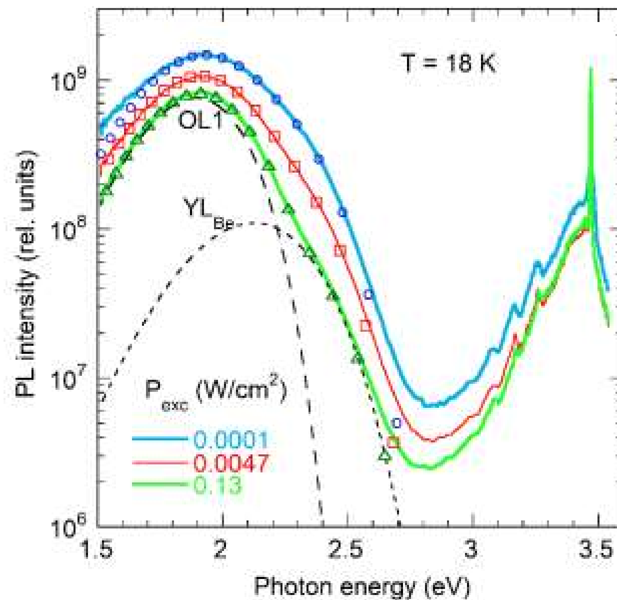

Figure 7. PL spectra from GaN:Be,F (sample u-12-13-1100) at T = 18 K and selected P_{exc}. The PL spectra are divided by P_{exc}. The dashed lines are calculated using Eq. (1) with parameters in Table 2 and $\Delta = -0.025$ eV for the YL_{Be} band and Δ = -0.005 eV for the OL1 band. The symbols show the sums of the simulated curves for the YL_{Be} and OL1 bands.

measured spectra, the shape of the OL1 band is found (the parameters are given in Table 2). The relative contribution of the YL_{Be} band decreases with increasing P_{exc} because of its earlier saturation. With increasing temperature, the quenching of the YL_{Be} band begins at about 170 K, while the intensity of the OL1 band does not show a substantial change up to 300 K (Figure 8).

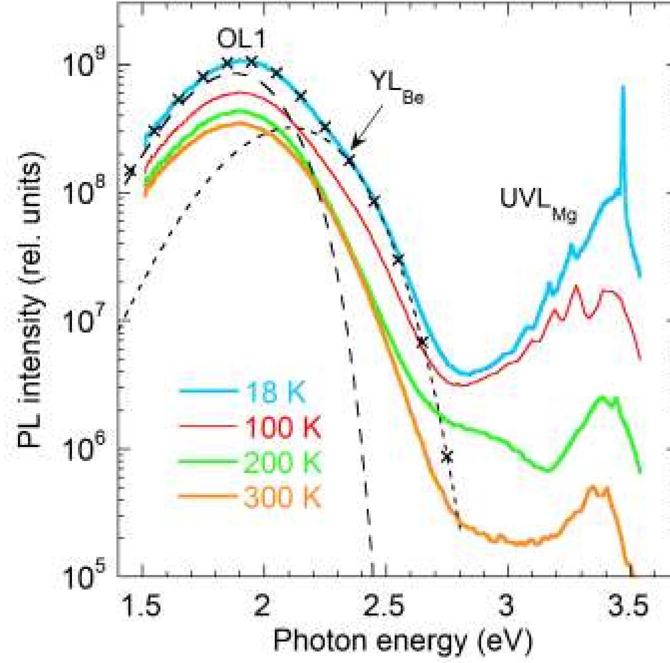

Figure 8. PL spectra from GaN:Be,F (sample u-12-13-1100) at P_{exc} = 0.0047 W/cm^2 and selected temperatures. The dashed lines are calculated using Eq. (1) with parameters in Table 2 and $\Delta = -0.04$ eV for the YL_{Be} band and Δ = -0.02 eV for the OL1 band. The × symbols show the sum of the simulated curves for the YL_{Be} and OL1 bands at T = 18 K.

The shape of the OL1 band was studied after subtracting the YL_{Be} band (Figure 9). The full width at half maximum (FWHM) increases with temperature and can be fitted with the following expression

$$W(T) = W(0)\sqrt{\coth\left(\frac{\hbar\cdot}{2kT}\right)}, \quad (4)$$

where W is the FWHM and $\hbar$ is the energy of the effective phonon mode in the excited state of the defect. From the best fit $\hbar$ = 50-60 meV is found.

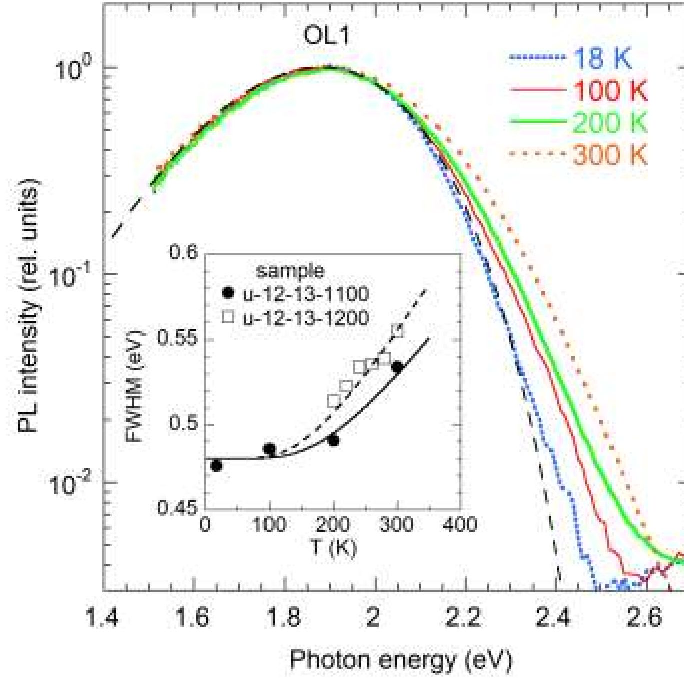

Figure 9. Normalized PL spectra from GaN:Be,F (sample u-12-13-1100) after subtracting the YL_{Be} band. The black dashed line is calculated using Eq. (1) with parameters in Table 2 and $\Delta = 0$ for the OL1 band. The inset shows the temperature dependence of the OL1 band FWHM. The lines in the inset are calculated using Eq. (4) with $\hbar$ = 60 meV (solid line) and 50 meV (dashed line).

In TRPL experiments, the OL1 decay curve $I^{PL}(t)$ at $T = 18$ K is nearly exponential at $t < 10^{-5}$ s after a laser pulse, with the characteristic lifetime $\tau \approx 4$ μs. In the time interval 10^{-5} -10^{-3} s, both the OL1 and YL_{Be} bands decay non-exponentially, approximately as $I^{PL}(t) \propto t^{-1}$.

3.5.2. The Red (RL5) Band in Conductive n-type GaN:Be,F

In PL spectra from six Si-doped GaN samples where the concentration of F significantly exceeds that of Be (Si-12-13 and Si-13-14 annealed at 1100, 1200, and 1300 °C), the OL1 band could not be found. However, in these samples, a broad red band (RL5) appeared as a shoulder to the YL_{Be} band (Figure 10). Unfortunately, our PL setup does not allow measuring PL spectra below 1.5 eV, and only the high-energy side of this band is observed.

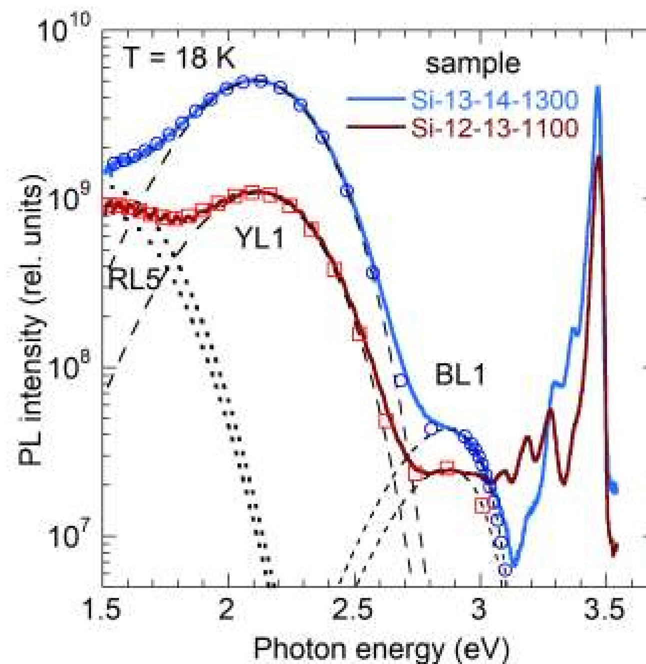

Figure 10. PL spectra from Si-doped GaN:Be,F with [F] > [Be]. T = 18 K and P_{exc} = 0.0001 W/cm^2. The dashed lines for are calculated using Eq. (1) with parameters in Table 2 and Δ = – 0.035 eV for the YL_{Be} band and Δ = 0.01 eV for the BL1 band. The dotted lines are Gaussian curves with $\hbar\omega_{max}$ = 1.50 eV and σ = 0.206 eV. The empty circles and squares show sums of the simulated curves for three PL bands.

3.5.3. PL from GaN Implanted with F

Two halves of 2-inch GaN/sapphire wafers were implanted with F ions only. Namely, undoped GaN grown by MOCVD and Si-doped GaN grown by HVPE on 2-inch sapphire substrates were

implanted at 600 °C with $^{19}F^+$ ions, cut into smaller samples and annealed in N_2 ambient at T_{ann} = 1100 and 1200 °C for 1 h (Series G in Table 1). PL from samples grown by MOCVD contained a strong YL1 band due to significant contamination with carbon. The intensity of the YL1 band in samples grown by HVPE was much lower. Figure 11 shows low-temperature PL spectra from two Si-doped GaN samples implanted with F and annealed at two temperatures.

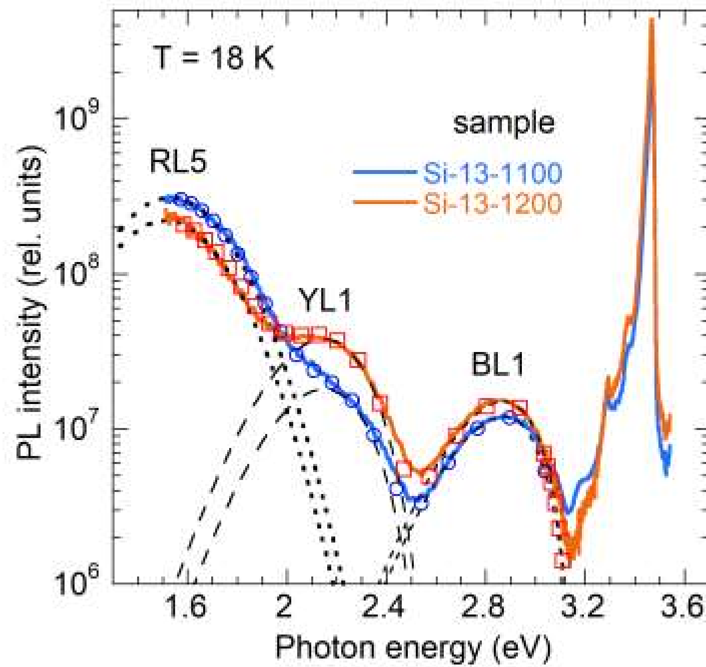

Figure 11. PL spectrum from conductive *n*-type GaN:F. T = 18 K and P_{exc} = 0.002 W/cm^2. The dashed lines are calculated using Eq. (1) with parameters in Table 2 and Δ = -0.01 eV for the YL1 and BL1 bands. The dotted lines are Gaussian curves with $\hbar\omega_{max}$ = 1.55 eV and σ = 0.206 eV. The empty circles show sums of the simulated curves for three PL bands.

In addition to relatively weak BL1 and YL1 bands, the spectra contain a strong red band labeled RL5. By fitting the shapes of the BL1 and YL1 bands and subtracting them from the spectra, we obtained the shape of the RL5 band. In Figure 11 it is fitted with a Gaussian curve (dotted line) for simplicity because only the high-energy side of the band can be detected in our setup. The shape

and position of the RL5 band in GaN implanted with F are very similar to the red band in GaN co-implanted with Be and F (Figure 10).

In undoped GaN grown by MOCVD and implanted with F, the YL1 band was the strongest PL band, at least at low excitation intensity (Figure 12). The ZPL of the YL1 band is found at 2.57 eV at $T = 18$ K and $P_{exc} = 5\times10^{-5}$ W/cm^2. However, with increasing excitation intensity, the YL1 band saturates, and the OL1 band can be resolved. After comparing PL spectra from GaN samples co-implanted with Be and F with GaN samples implanted with only F, we conclude that the OL1 and RL5 bands in GaN:Be,F and GaN:F are unrelated to Be.

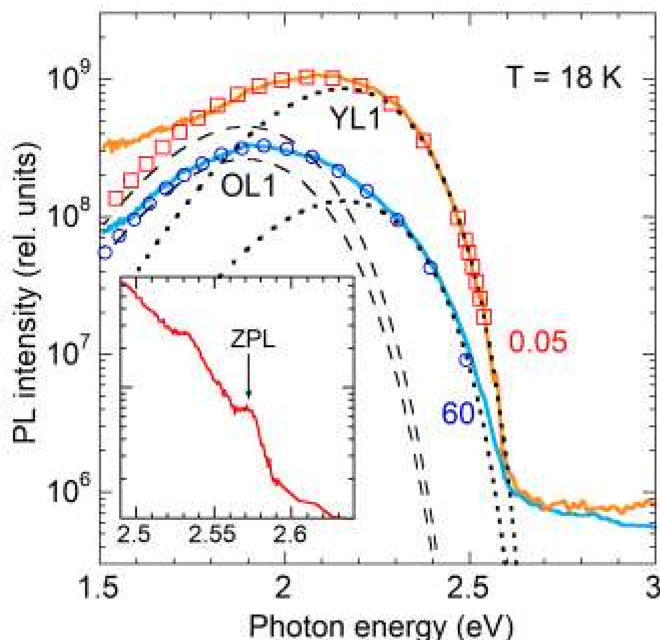

Figure 12. PL spectra from GaN:F (sample u-13-1100) at $T = 18$ K. The PL intensity is divided by excitation intensity ($P_{exc} = 60$ and 0.05 mW/cm^2 as indicated). The dotted and dashed lines are calculated using Eq. (1) with parameters in Table 2 for the YL1 (dotted lines) and the OL1 band (dashed lines). The empty circles show sums of the simulated curves for the OL1 and YL1 bands. The inset zooms in the region where the ZPL of the YL1 band at 2.57 eV is observed.

4. Discussion

The UVL_{Be} band is usually observed in semi-insulating GaN:Be samples. This can be explained by the fact that thermal annealing is required to activate the shallow Be_{Ga} state.[27] The activation is associated with the removal of hydrogen from GaN. It is well-known that hydrogen ions (H^+) diffuse readily at $T > 600$ °C in semi-insulating or p-type GaN, whereas no diffusion is observed at least up to $T = 1050$ °C in conductive n-type GaN because hydrogen is negatively charged (H^-) in such material.[36-40] This explains why the UVL_{Be} band was not observed in n-type GaN:Be grown by MBE and MOCVD techniques and annealed at 800-900 °C.[2,3] Here, for the first time, the UVL_{Be} band was discovered in conductive n-type GaN:Be,F annealed at 1200 and 1300 °C. Note that the UVL_{Be} band was not found in samples annealed at a lower temperature (Si-13-13-1100). This indicates that activation of the UVL_{Be} band in conductive n-type GaN (presumably caused by out-diffusion of hydrogen) becomes possible at annealing temperatures of 1200 °C and higher.

For conductive n-type GaN, the rate equation model allows finding important parameters of defects responsible for PL bands, such as electron- and hole-capture coefficients.[28,42,43] The electron capture coefficient for the UVL_{Be} band ($C_n \approx 10^{-11}$ cm^3/s) is the largest among acceptors in GaN (the second largest is the shallow Mg_{Ga} acceptor with $C_n = 3.2\times10^{-12}$ cm^3/s).[28] For the YL_{Be} band, $C_n = 1\times10^{-13}$ cm^3/s. The hole-capture coefficient is determined from the temperature dependence of the SSPL. For the UVL_{Be} band, this coefficient is found with a considerable uncertainty ($C_p = (1\text{-}20)\times10^{-7}$ cm^3/s). Generally, lower transition levels result in larger carrier capture coefficients, which is true for the values of C_n above. Then the value of C_p for the UVL_{Be} band of $\sim10^{-6}$ cm^3/s is likely the lower bound. This value agrees with typical C_p for acceptors that efficiently capture holes in n-type GaN.[28] In particular, $C_p = 1\times10^{-6}$ cm^3/s for the Mg_{Ga}-related

UVL_{Mg} band and $C_p \approx 4\times10^{-7}$ cm^3/s for the YL_{Be} band. The large C_p and C_n for the UVL_{Be} band agree with the earlier assumptions [1,3] that it is caused by a shallow acceptor.

The concentration of the YL_{Be}-related defects is close to the Be concentration.[2] We earlier attributed the UVL_{Be} and YL_{Be} bands to the shallow and deep states of the same defect (the Be_{Ga} acceptor).[2] However, such attribution leaves several questions unanswered. In particular, why is the UVL_{Be} and YL_{Be} intensities ratio not the same in different GaN:Be samples, and why is the YL_{Be} band intense already before the annealing, while the UVL_{Be} band requires annealing-induced activation? The concentration of defects responsible for the UVL_{Be} band is typically lower by several orders of magnitude than that for the YL_{Be} band. At the same time, the hole capture coefficients for these two bands are similar. Our recent studies of MOCVD-grown GaN:Be, to be reported elsewhere,[41] provide strong evidence that the YL_{Be} band is caused by the isolated Be_{Ga} defect. As for the UVL_{Be} band, we preliminarily propose that this is the Be_{Ga} acceptor trapped at some external defects such as dislocations. This shallow state is highly susceptible to the presence of hydrogen and possibly other disturbances that cause local electric fields. More studies are needed to elucidate these questions.

Co-implantation of GaN with Be and F at T = 600 °C and subsequent annealing at 1100-1300 °C for 30-60 min obstructed formation of nitrogen vacancies. Such a conclusion follows from the absence of the RL_{Be} band responsible for the $Be_{Ga}V_N$ complex and the rarely-observed weak GL2 band responsible for the isolated V_N defect. This result agrees with the results of Takahashi *et al*.[8] They concluded that the V_N defects disappear in Mg-implanted GaN after additional implantation with F. Note that for GaN implanted with only Be and annealed at 1100 °C for 4 hours, the GL2 and RL_{Be} bands were found. [18]

Two new PL bands are discovered in this study: the OL1 band with a maximum at 1.9 eV and the RL5 band with a maximum at 1.5 eV. The implantation of GaN with Be and F produces the OL1 band in samples with a low concentration of free electrons and the RL5 band in Si-doped conductive *n*-type GaN. GaN implanted with only F reveals very similar bands, suggesting that they are unrelated to Be. One may expect that these PL bands are caused by defects involving F atoms or their complexes with native defects created during implantation. For example, our HSE calculations suggest that the F_NV_{Ga} complex could be a good candidate for the defect responsible for the OL1 band, with computed PL maximum and ZPL at 1.98 and 2.50 eV, respectively, for the transition via 0/+ level. However, our preliminary studies of GaN implanted with Cl ions show PL spectra similar to the ones from F-implanted GaN. Further investigations are needed to confirm or reject the relation of the OL1 and RL5 bands to defects involving F or Cl.

5. Conclusion

The sequential implantation of Be and F ions into GaN at T = 600 °C and annealing in ambient-pressure nitrogen at T = 1100-1300 °C reduced the concentration of nitrogen vacancies. New defect-related bands (labeled OL1 and RL5) appeared in the PL spectrum in samples co-implanted with F and Be and samples implanted with only F ions. For the first time, the UVL_{Be} band from the shallow Be-related acceptor is observed in conductive *n*-type GaN. To activate this PL band in *n*-type GaN, relatively high annealing temperatures are required. The electron- and hole-capture coefficients for the related defect are 10^{-13} and ~10^{-7}-10^{-6} cm^3/s, respectively.

6. Methods

6.1. Samples

Nominally undoped GaN (samples with the prefix "u") and Si-doped GaN layers (prefix "Si") were grown on 2-inch sapphire substrates by HVPE at Kyma Technology. The samples were implanted at 600 °C with different doses and energies of $^{9}Be^{+}$ and $^{19}F^{+}$ ions at a 7° tilt angle (Table 1). Some samples were implanted with only F. In this case, Si-doped GaN grown by HVPE and undoped GaN grown by MOCVD were used. The ion profiles were simulated with the Transport of Ions in Matter (TRIM) software and verified for selected samples with secondary ion mass spectrometry (SIMS) measurements. The concentration of Si in HVPE Si-doped GaN is about 3×10^{18} cm^{-3} and that in undoped GaN is below our SIMS detection limit (~10^{17} cm^{-3}).

After implantation, the samples were cut into 5×5 mm squares and annealed in N_2 ambient at T_{ann} = 1100 and 1200 °C for 1 h and at T_{ann} = 1300 °C for 1 h. A protective ~80 nm-thick AlN cap layer was deposited onto the sample surface before the implantation and removed after the annealing. The Be- and F-ion energy was 40 and 95 keV, respectively, to provide a similar implantation profile for both impurities, with a maximum at ~100 nm, which is the optimal depth for PL experiments.

6.2. Measurement Details

SSPL was excited with a HeCd laser at 325 nm, dispersed by a 1200 rules/mm grating in a 0.3-m monochromator, and detected by a cooled photomultiplier tube. TRPL was excited with a pulsed nitrogen laser and analyzed with an oscilloscope. A closed-cycle optical cryostat was used for temperatures between 18 and 320 K. The IQE for each PL band, η_i, was found by comparing the intensity after integrating over the PL band with that from calibrated GaN samples.[28,42,43] Other details of PL experiments can be found elsewhere.[28,44] The as-measured PL spectra were

corrected for the measurement system's spectral response, and PL intensity was additionally multiplied by λ^3, where λ is the light wavelength, to present the PL spectra in units proportional to the number of emitted photons as a function of photon energy.[28,44]

6.3. Calculation Details

Theoretical calculations were performed using the HSE hybrid functional.[45] The HSE functional used in this work was tuned to fulfill the generalized Koopmans' condition for the localized acceptor states of the F_i and F_iBe_{Ga} defects (fraction of exact exchange is 0.24, the range separation parameter is 0.2 $Å^{-1}$). Tests show that this parametrization also fulfills Koopmans' condition for the localized states of F_NV_{Ga} and F_{Ga} defects to within 0.02 eV. For the shallow donor defects, the delocalized defect states are resonant with the conduction band for which Koopmans' condition holds. Calculations were performed in 300-atom hexagonal supercells at the Γ-point, with plane-wave energy cutoffs of 500 eV. All defect atomic structures were relaxed using HSE to minimize forces to 0.05 eV/Å or less. Artificial electrostatic interactions in calculated total energies (in both HSE Koopmans' tuning and formation energy calculations) were corrected using the Lany-Zunger approach,[46] which appears to perform well, particularly for HSE tuning purposes.[47] The incorporation of F- and Be-containing defects into GaN is determined by the elemental chemical potentials μ_F, μ_{Be}, μ_{Ga}, and μ_N. Since in our case F and Be are implanted into grown GaN samples, with subsequent annealing at 1100-1300 °C in N_2 ambient, the formation of defects is assumed to be limited by the N-rich conditions. In this case, the chemical potential of nitrogen is set to $\mu_N(N_2)$, while that of gallium is set to $\mu_{Ga}(\text{Ga metal}) + \Delta H_f(\text{GaN})$, where $\Delta H_f(\text{GaN})$ is the formation enthalpy of GaN, with HSE calculated value of -1.17 eV. During annealing in N_2 ambient, the formation of Be- and F-related defects is assumed to be limited by Be_3N_2 and NF_3, respectively.

Acknowledgements

The work at VCU and SUNY was supported by the National Science Foundation under grants DMR-1904861 and DMR-1905186, respectively.

Conflict of Interest

The authors have no conflicts to disclose.

Data Availability Statement

The data supporting this study's findings are available from the corresponding author upon reasonable request.

Keywords

Photoluminescence, GaN, point defects, complexes, ion implantation, semiconductors.

References

[1] D. O. Demchenko, M. Vorobiov, O. Andrieiev, T. H. Myers, and M. A. Reshchikov, "Shallow and deep states of beryllium acceptor in GaN: Why photoluminescence experiments do not reveal small polarons for defects in semiconductors", *Phys. Rev. Lett*. **126**, 027401 (2021).

[2] M. A. Reshchikov, M. Vorobiov, O. Andrieiev, B. McEwen, E. Rocco, V. Meyers, D. O. Demchenko, and F. Shahedipour-Sandvik, "Photoluminescence from Be-Doped GaN Grown by Metal-Organic Chemical Vapor Deposition", *Phys. Stat. Sol.* (b) 202200487 (2022).

[3] M. Vorobiov, O. Andrieiev, D. O. Demchenko, and M. A. Reshchikov, "Point Defects in Beryllium Doped GaN", *Phys. Rev B* **104**, 245203 (2021).

[4] S. Sugita, Y. Watari, G. Yoshizawa, J. Sodesawa, H. Yamamizu, K.-T. Liu, Y.-K. Su, and Y. Horikoshi, "Growth of Be-doped p-type GaN under invariant polarity conditions", *Jpn. J. Appl. Phys.* **42**, 7194-7197 (2003).

[5] Z.-C. Feng, Y. J. Sun, L. S. Tan, S. J. Chua, J. W. Yu, C. C. Yang, W. Lu, and W. E. Collins, "P-type doping in GaN through Be implantation", *Phys. Stat. Sol*. (*c*) **2**, 2415-2419 (2005).

[6] C.-C. Yu, C.-F. Chu, J.-Y. Tsai, C.-F. Lin, W.-H. Lan, C.-I. Chiang, and S.-C. Wang, "Be-implanted p-type GaN with high carrier concentration", *Jap. J. Appl. Phys*. **40**, L417-L419 (2001).

[7] Y. Nakano, T. Kachi, and T. Jimbo, "Effect of Be^{+} + O^{+} co-implantation on Be acceptors in GaN", *Appl. Phys. Lett*. **82**, 2082-2084 (2003).

[8] M. Takahashi, A. Tanaka, Y. Ando, H. Watanabe, M. Deki, M. Kushimoto, S. Nitta, Y. Honda, K. Shima, K. Kojima, S. F. Chichibu, and H. Amano, "Impact of high-temperature implantation of Mg ions into GaN", *Jap. J. Appl. Phys*. **59**, 056502 (2020).

[9] M. Takahashi, A. Tanaka, Y. Ando, H. Watanabe, M. Deki, M. Kushimoto, S. Nitta, Y. Honda, K. Shima, K. Kojima, S. F. Chichibu, K. J. Chen, and H. Amano, "Suppression of Green Luminescence of Mg-Ion-Implanted GaN by Subsequent Implantation of Fluorine Ions at High Temperature", *Phys. Stat. Sol. B* **257**, 1900554 (2020).

[10] H. Sakurai, T. Narita, K. Kataoka, K. Hirukawa, K. Sumida, S. Yamada, K. Sierakowski, M. Horita, N. Ikarashi, M. Bockowski, J. Suda, and T. Kachi, "Effects of the sequential implantation of Mg and N ions into GaN for p-type doping", *Appl. Phys. Express* **14**, 111001 (2021).

[11] K. Shima, A. Tanaka, S. Takashima, K. Ueno, M. Edo, K. Kojima, A. Uedno, S. Ishibashi, and S. F. Chichibu, "Improved minority carrier lifetime in p-type GaN segments prepared by vacancy-guided redistribution of Mg", *Appl. Phys. Lett*. **119**, 182106 (2021).

[12] V. Meyers, E. Rocco, K. Hogan, B. McEwen, M. Shevelev, V. Sklyar, K. Jones, M. Derenge, and F. Shahedipour-Sandvik, "P-type conductivity and suppression of green luminescence in Mg/N co-implanted GaN by gyrotron microwave annealing", *J. Appl. Phys*. **130**, 085704 (2021);

[13] M. A. Reshchikov, D. O. Demchenko, J. D. McNamara, S. Fernández-Garrido, and R. Calarco, "Green luminescence in Mg-doped GaN", *Phys. Rev. B* **90**, 035207 (2014).

[14] K. Kojima, S. Takashima, M. Edo, K. Ueno, M Shimizu, T. Takahashi, S. Ishibashi, and S. F. Chichibu, "Nitrogen vacancies as a common element of the green luminescence and

nonradiative recombination centers in Mg-implanted GaN layers formed on a GaN substrate", *Appl. Phys. Express* **10**, 061002 (2017).

[15] M. A. Reshchikov, "Photoluminescence from Vacancy-Containing Defects in GaN", *Phys. Stat. Sol.* (b) 202200402 (2022).

[16] M. Horita, T. Narita, T. Kachi, and J. Suda, "Nitrogen-displacement-related electron traps in n-type GaN grown on a GaN freestanding substrate", *Appl. Phys. Lett.* **118**, 012106 (2021).

[17] M. Endo, M. Horita, and J. Suda, "Hole traps related to nitrogen displacement in p-type GaN grown by metalorganic vapor phase epitaxy on freestanding GaN", *Appl. Phys. Lett.* **120**, 142104 (2022).

[18] M. A. Reshchikov, O. Andrieiev, M. Vorobiov, D. Ye, D. O. Demchenko, K. Sierakowski, M. Bockowski, B. McEwen, V. Meyers, and F. Shahedipour-Sandvik, "Thermal annealing of GaN implanted with Be", *J. Appl. Phys*. **131**, 125704 (2022).

[19] K.-H. Hong, I. H. Hwang, H. S. Choi, J. Oh, J. Shin, U.-I. Chung, and J. Kim, "Impacts of fluorine on GaN high electron mobility transistors: Theoretical study", *Phys. Stat. Sol. PRL* **4**, 332-334 (2010).

[20] A. Janotti, E. Snow, and C. G. Van de Walle, "A pathway to p-type wide-bandgap semiconductors", *Appl. Phys. Lett*. **95**, 172109 (2009).

[21] J. Lu, M. Gao, J. Zhang, Y. Wang, and Z. Yu, "First-principles calculations of effects of Fluorine impurity in GaN", in *SISPAD: 2008 International Conference on Simulation of Semiconductor Processes and Devices*, IEEE, New York, 2008, pp. 233-236. 10.1109/SISPAD.2008.4648280

[22] R. Wang, W. Tan, J. Zhang, F.-X. Chen, and S.-H. Wei, "First-principles study of alloying effects on fluorine incorporation in AlxGa1-xN alloys", *J. Phys. D: Appl. Phys.* **51**, 065108 (2018).

[23] R. Jakiela, K. Sierakowski, T. Sochacki, M. Iwinska, M. Fijalkowski, A. Barcz, and M. Bockowski, "Investigation of diffusion mechanism of beryllium in GaN", *Physica B* **594**, 412316 (2020).

[24] M. J. Wang, L. Yuan, K. J. Chen, F. J. Xu, and B. Shen, “Diffusion mechanism and thermal stability of fluorine ions in GaN after ion implantation”, *J. Appl. Phys*. **105**, 083519 (2009).

[25] M. J. Wang, L. Yuan, C. C. Chen, C. D. Beling, and K. J. Chen, “Defect formation and annealing behaviors of fluorine-implanted GaN layers revealed by positron annihilation spectroscopy”, *Appl. Phys. Lett*. **94**, 061910 (2009).

[26] U. Wahl., J. G. Correia, A. R. G. Costa, T. A. L. Lima, J. Moens, M. J. Kappers, M. R. sa Silva, L. M. C. Pereira, and A. Vantomme, “Direct evidence of Be as an amphoteric dopant in GaN”, *Phys. Rev. B* **105**, 184112 (2022).

[27] D. O. Demchenko and M. A. Reshchikov, “Hydrogen passivation of the beryllium acceptor in GaN and a possible route for *p*-type doping”, *Appl. Phys. Lett*. **118**, 142103 (2021).

[28] M. A. Reshchikov, “Measurement and analysis of photoluminescence in GaN”, *J. Appl. Phys*. **129**, 121101 (2021).

[29] B. McEwen, M. A. Reshchikov, E. Rocco, V. Meyers, K. Hogan, O. Andrieiev, M. Vorobiov, D. O. Demchenko, and F. Shahedipour-Sandvik, “MOCVD Growth and Characterization of Be-Doped GaN”, *ACS Applied Electronic Materials* **4**, 3780-3785 (2022).

[30] M. A. Reshchikov, D. O. Demchenko, M. Vorobiov, O. Andrieiev, B. McEwen, F. Shahedipour-Sandvik, K. Sierakowski, P. Jaroszynski, and M. Bockowski. “Photoluminescence related to Ca in GaN”, *Phys. Rev. B* **106**, 035206 (2022).

[31] M. A. Reshchikov, “Giant shifts of photoluminescence bands in GaN”, *J. Appl. Phys*. **127**, 055701 (2020).

[32] M. A. Reshchikov, “Time-resolved photoluminescence from defects in GaN”, *J. Appl. Phys*. **115**, 103503 (2014).

[33] M. A. Reshchikov, J. D. McNamara, M. Toporkov, V. Avrutin, H. Morkoç, A. Usikov, H. Helava, and Yu. Makarov, “Determination of the electron-capture coefficients and the concentration of free electrons in GaN from photoluminescence”, *Scientific Reports* **6**, 37511 (2016). doi:10.1038/srep37511

[34] D. Wickramaratne, C. E. Dreyer, B. Monserrat, J.-X. Shen, J. L. Lyons, A. Alkauskas, and C. G. Van de Walle, "Defect identification based on first-principles calculations for deep level transient spectroscopy", **113**, 192106 (2018).

[35] M. A. Reshchikov and R. Y. Korotkov, "Analysis of the temperature and excitation intensity dependencies of photoluminescence in undoped GaN films", Phys. Rev. B **64**, 115205 (2001).

[36] W. Gotz, N. M. Johnson, J. Walker, D. P. Bour, and R. A. Street, "Activation of acceptors in Mg-doped GaN grown by metalorganic chemical vapor deposition", *Appl. Phys. Lett*. **68**, 667-669 (1996).

[37] R. Czernecki, E. Grzanka, R. Jakiela, S. Grzanka, C. Skierbiszewski, H. Turski, P. Perlin, T. Suski, K. Donimirski, and M. Leszczynski, "Hydrogen diffusion in GaN:Mg and GaN:Si", *J. Alloys and Compounds* **747**, 354-358 (2018).

[38] S. Limpijumnong and C. G. Van de Walle, "Stability, diffusivity, and vibrational properties of monoatomic and molecular hydrogen in wurtzite GaN", *Phys. Rev. B* **68**, 235203 (2003).

[39] M. A. Reshchikov, D. O. Demchenko, D. Ye, O. Andrieiev, M. Vorobiov, K. Grabianska, M. Zajac, P. Nita, M. Iwinska, M. Bockowski, B. McEwen, and F. Shahedipour-Sandwik, "The effect of annealing on photoluminescence from defects in ammonothermal GaN", *J. Appl. Phys*. **131**, 035704 (2022).

[40] M. A. Reshchikov, O. Andrieiev, M. Vorobiov, B. McEwen, F. Shahedipour-Sandvik, D. Ye, and D. O. Demchenko, "Stability of the C_NH_i complex and the BL2 luminescence band in GaN", *Phys. Stat. Sol*. (*b*) **258**, 2100392 (2021).

[41] M. A. Reshchikov, M. Vorobiov, O. Andrieiev, D. O. Demchenko, B. McEwen, and F. Shahedipour-Sandwik, "Dual Nature of the Be_{Ga} Acceptor in GaN: Evidence from Photoluminescence", submitted to *Phys*. Rev. B.

[42] M. A. Reshchikov, M. A. Foussekis, J. D. McNamara, A. Behrends, A. Bakin, and A.Waag, "Determination of the absolute internal quantum efficiency of photoluminescence in GaN co-doped with Zn and Si", *J. Appl. Phys*. **111**, 073106 (2012).

[43] M. A. Reshchikov, A. A. Kvasov, M. F. Bishop, T. McMullen, A. Usikov, V. Soukhoveev, and V. A. Dmitriev, "Tunable and abrupt thermal quenching of photoluminescence in high-resistivity Zn-doped GaN", *Phys. Rev. B* **84**, 075212 (2011).

[44] M. A. Reshchikov, M. Vorobiov, D. O. Demchenko, Ü. Özgür, H. Morkoç, A. Lesnik, M. P. Hoffmann, F. Hörich, A. Dadgar, and A. Strittmatter, "Two charge states of the C_N acceptor in GaN: Evidence from photoluminescence", *Phys. Rev. B* **98**, 125207 (2018).

[45] J. Heyd, G. E. Scuseria, and M. Ernzerhof, "Hybrid functionals based on a screened Coulomb potential", *J. Chem. Phys*. **118**, 8207-8215 (2003)

[46] S. Lany and A. Zunger, "Assessment of correction methods for the band-gap problem and for finite-size effects in supercell defect calculations: Case studies for ZnO and GaAs" *Phys. Rev. B* **78**, 235104 (2008).

[47] D. O. Demchenko and M. A. Reshchikov, "Koopmans' tuning of HSE hybrid density functional for calculations of defects in semiconductors: A case study of carbon acceptor in GaN, *J. Appl. Phys*. **127**, 155701 (2020).